Geophysical Research Letters

RESEARCH LETTER
10.1029/2023GL104818

Impact-Induced Seafloor Deformation From Submarine Landslides: Diagnostic of Slide Velocity?

Brandi L. Lenz[1,2], W. Ashley Griffith[1], and Derek E. Sawyer[1]

[1]School of Earth Sciences, The Ohio State University, Columbus, OH, USA, [2]Department of Geology and Geophysics, Texas A&M University, College Station, TX, USA

Key Points:

- A broad zone of impact-induced deformation is observed immediately adjacent to the massive 44-N Slide offshore Oregon
- The deformation of seafloor sediments observed at the slide terminus requires slide deceleration, implying catastrophic emplacement
- Modeled impact forces require a slide velocity of up to 60 m/s, which may have been sufficient to generate a tsunami

Supporting Information:

Supporting Information may be found in the online version of this article.

Correspondence to:

D. E. Sawyer,
sawyer.144@osu.edu

Citation:

Lenz, B. L., Griffith, W. A., & Sawyer, D. E. (2023). Impact-induced seafloor deformation from submarine landslides: Diagnostic of slide velocity? *Geophysical Research Letters*, *50*, e2023GL104818. https://doi.org/10.1029/2023GL104818

Received 8 JUN 2023
Accepted 25 JUL 2023

Author Contributions:

Conceptualization: Brandi L. Lenz, W. Ashley Griffith, Derek E. Sawyer
Data curation: Brandi L. Lenz
Formal analysis: Brandi L. Lenz, W. Ashley Griffith
Funding acquisition: Derek E. Sawyer
Investigation: Brandi L. Lenz, W. Ashley Griffith
Methodology: Brandi L. Lenz, W. Ashley Griffith
Resources: Brandi L. Lenz, W. Ashley Griffith
Software: Brandi L. Lenz, W. Ashley Griffith

Abstract Submarine landslides shape continental margins, transfer massive amounts of sediment downslope, and can generate deadly and destructive tsunamis. Submarine landslides are common globally, yet constraining hazard potential of future events is limited by a short historical record and a wide range of possible slide dynamics. We test a novel approach to investigate slide dynamics using properties of the deformation zone induced by a large submarine landslide along the Cascadia margin, offshore Oregon. We use a simple model of a line load on a poroelastic half space to show the deformation zone size required rapid transport and deceleration. We argue that the slide moved at high speeds, aided by low dynamic frictional resistance, suggesting this event could have generated a tsunami. This method is applicable where slide-induced impact zones are observed.

Plain Language Summary The Cascadia margin is susceptible to underwater landslides and tsunami hazards due to the active subduction zone that can produce large magnitude earthquakes. However, determining whether future submarine landslides will be tsunamigenic is challenging. While past landslide deposits can easily be identified and in many cases age-dated, the dynamic process including the initial acceleration and velocity that created the deposit is almost never known. We present a novel approach to back-analyze slide velocity of past landslides by using the characteristics of the deformation zone that occurred when the landslide deposit came to rest on the seafloor. Our models suggest that the slide hydroplaned while moving at high-speeds (up to 60 m/s) with a run-out distance of 10-km from the source, which match the observations. While our method does not model tsunamis explicitly, the high speeds are consistent with known tsunamigenic slides. This approach provides critically important constraints on the slide velocity and therefore the hazards of submarine landslides that can occur at Cascadia.

1. Introduction

Submarine landslides have the potential to create and/or amplify earthquake-induced tsunamis (Hampton et al., 1996; Harbitz, 1992; Harbitz et al., 2014; Jiang & LeBlond, 1992; Kawata et al., 1999; Locat & Lee, 2002; Masson et al., 2006; ten Brink, 2009; Vanneste et al., 2013; von Huene et al., 1989). Examples of submarine landslide-induced tsunamis that resulted in large wave run-up heights and numerous fatalities include the 1929 Grand Banks event (13-m run-up, 28 deaths) (Fine et al., 2005; Løvholt et al., 2019), 1992 Flores event (up to 26-m run-up, 2,080 deaths) (Yeh et al., 1993), 1998 Papa New Guinea event (>15-m run-up, 2,200 deaths) (Tappin et al., 2002), and the more recent 2018 Palu Bay event (6-m run-up, >2,000 deaths) (Muhari et al., 2018; Pakoksung et al., 2019).

Not all submarine landslides generate tsunami (Løvholt et al., 2017). A major challenge in evaluating potential hazard of submarine landslides is the relative infrequency of tsunamigenic landslides in any region compared to the duration of recorded history. Similar to earthquake hazards assessment, the historical record can be extended by interrogating the geologic record of ancient landslides (e.g., Goldfinger et al., 2012; Howarth et al., 2021; Kioka et al., 2019; McHugh et al., 2016; Mountjoy et al., 2018; Rowe & Griffith, 2015; Wallace, 1981). However, a critical challenge is that interpreting the rate of landslide motion based on the structure of landslide deposits is difficult. Initial acceleration (Grilli & Watts, 2005; Haugen et al., 2005; Løvholt et al., 2005) and the maximum velocity (Tinti et al., 2001; Ward, 2001) are the biggest influences on tsunami generation from submarine landslides; therefore, the ability to identify diagnostic features of rapid submarine landslide motion in the structure of landslide deposits and related deformation would represent a major advance in the evaluation of tsunamigenic

Validation: Brandi L. Lenz, W. Ashley Griffith
Visualization: Brandi L. Lenz, W. Ashley Griffith
Writing – original draft: Brandi L. Lenz, Derek E. Sawyer
Writing – review & editing: Brandi L. Lenz, W. Ashley Griffith, Derek E. Sawyer

hazard assessment. Here, we evaluate the slide velocity potential of the 44-N slide offshore Oregon based on deformation structures in sediments near the terminus of the slide blocks.

The Cascadia subduction zone occurs along the Pacific margin of North America. The Juan de Fuca, Gorda, and Explorer plates are actively subducting beneath the North American plate at rates of ∼30–45 mm/yr (McCaffrey et al., 2013). Cascadia is seismically active and estimated to produce megathrust earthquakes about once every 500 years (Goldfinger et al., 2017; Walton et al., 2021). The Oregon margin has a long history of slope failures ranging from small non-cohesive slides to massive blocky slides (Goldfinger et al., 2000; Hill et al., 2022; Lenz & Sawyer, 2021; Lenz et al., 2019; McAdoo & Watts, 2004; McAdoo et al., 2000; Tréhu et al., 2022). Cascadia is therefore susceptible to many geohazards, including submarine landslides (Hill et al., 2022).

The 44-N slide is a large and blocky style submarine landslide, that is readily observable on the modern-day seafloor (Lenz et al., 2019) (Figure 1). Blocks of the 44-N landslide descended a 1,200 m drop along an approximately 13° slope, and 10 km horizontally to where they were deposited across a 100 km^2 area of the abyssal plain adjacent to the slope (Figure 1). The blocks are angular and rise up to 400-m above the surrounding seafloor, and their cohesion distinguishes them from debris flows (Figure 1). A distinguishing characteristic of this event is a conspicuous deformation zone immediately seaward of the landslide blocks (Figures 1 and 2) (Lenz et al., 2019). The deformation zone consists of a series of imbricate thrust sheets that accommodated horizontal shortening and vertical thickening of the sediments at the terminus of the slide blocks. The deformation zone is 275 m thick, 10 km long, and represents approximately 8% horizontal shortening (Lenz et al., 2019).

In this study we test the hypothesis that the 44-N Slide impacted the seafloor with sufficient forces to have created the deformation zone. To that end, we ask the question of whether the deformed sediments at the slide terminus could result from slow creep caused by the weight of the slide blocks, or if lateral momentum from decelerating slide blocks is required. We do this by examining the subsurface stress fields induced in a saturated, undrained poroelastic half space below the ocean bottom subjected to a line load along the half space surface. We examine the contributions of the weight of the slide blocks as well as shear tractions that would have resulted from frictional resistance during deceleration of the blocks. We then model slide transport with a ramp-flat slide geometry following the approach of Hürlimann et al. (2000) as an independent check on whether rapid transport is consistent with the observed final position of the slide blocks. Finally, we examine the validity and limitations of our approach and discuss implications for the 44-N slide as well as the broader applicability.

2. Methods

2.1. Line Loading of a Saturated, Undrained Poroelastic Half Space

We study deformation induced in the subsurface by a line load on a poroelastic half space (e.g., Johnson, 1985) situated at the ocean bottom. The full solution for the total stress state σ_{ij}^{T} results from the superposition of (A) the background stress state σ_{ij}^{o} arising from body forces induced by the overlying oceanic water column, the rock/sediment column beneath the ocean floor, hydrostatic pore fluid pressure, and Biot coupling between the poroelastic medium and pore fluids in the subsurface as described further below, and (B) the stress perturbation $\Delta\sigma_{ij}$ introduced by the landslide blocks at the surface (Figure 2a). Stresses are calculated in a cartesian coordinate system in which the half-space is located at depths $z \geq 0$, and the origin is located on the ocean bottom, 3,000 m below local sea level. All stresses are calculated in a tensor sign convention, with tension positive.

The background stress state accounts for the pore fluid pressure (P_f), overburden stress (σ_{zz}^{0}), and the horizontal stress (σ_{xx}^{0}) assuming a saturated and undrained isotropic, linear poro-elastic material (Figure 3). The pore fluid pressure is the sum of the pressure from the overlying oceanic water column above the seafloor and the pressure from the fluid within the pore space of the sediments (Equation 1) where seawater density (ρ_w) is 1,024 kg/m^3 and water depth D_w = 3,000 m. The overburden effective stress σ_{zz}^{0} is the sum of the pressure from the overlying sediment, the overlying water column, and the pore fluid pressure (Equation 2) where the bulk sediment density ρ_s = 1,800 kg/m^3 based on physical properties measured from nearby cores (Lenz et al., 2019; Shipboard Scientific Party, 1973). The horizontal effective stress σ_{xx}^{0} (Equation 3) is calculated assuming a state of perfect confinement (i.e., zero horizontal volumetric strain) and includes the effect of the Biot coefficient, which describes the change in volume in the poroelastic medium due to a change in pore pressure. We assume a Poisson's ratio ν = 0.25, resulting in the ratio $\frac{\nu}{1-\nu} \approx 0.33$, consistent with the expectation that in normally consolidated marine sediments

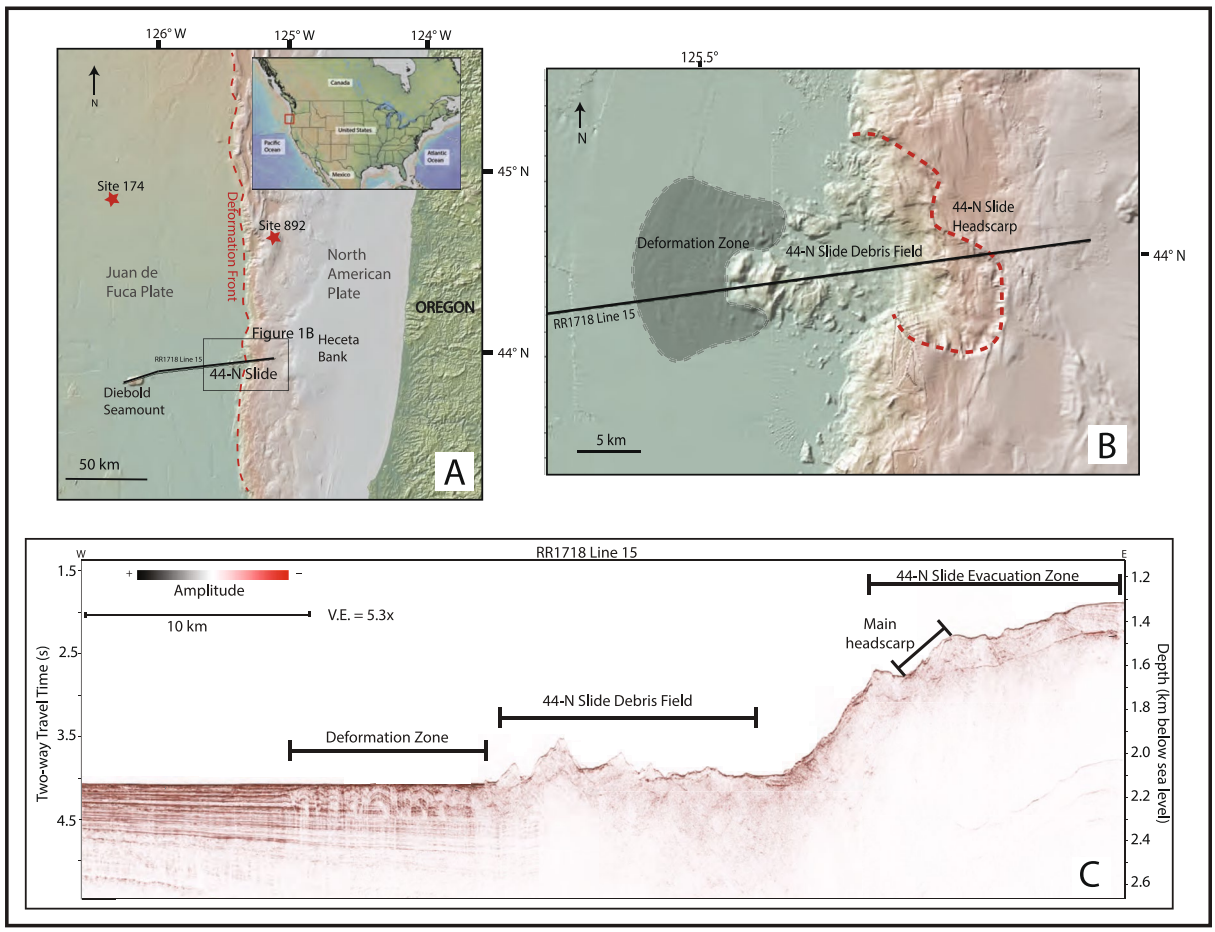

Figure 1. (a) Map of the Cascadia subduction zone offshore Oregon with seismic line 15 from cruise RR1718 that was used in this study. Red stars represent locations of Site 174 from DSDP Leg 18 (Shipboard Scientific Party, 1973) and Site 892 from ODP Leg 146 (Shipboard Scientific Party, 1994). Water depths here range from approximately 3,000 (cool colors) to 0-m at the coastline. Bathymetry created using the Global Multi-Resolution Topography (GMRT) database from http://www.geomapapp.org (Ryan et al., 2009). (b) Map view of area containing eastern half of seismic line 15 from cruise RR1718, showing prominent head scarp from 44-N slide, associated debris field containing many large blocks, and interpreted in situ deformation zone interpreted to be formed by the blocks. Water depths here range from approximately 3,000 (cool colors) to 1,300-m (warm colors). Bathymetry created using GMRT database from http://www.geomapapp.org (Ryan et al., 2009). (c) Eastern half of seismic line 15 from cruise RR1718 in panel (b)showing the main head scarp within a broader evacuation zone, blocks within 44-N Slide debris field, and associated frontal deformation zone modified from Lenz et al. (2019). (d) Close-up image of deformation zone (adapted from Lenz et al. (2019)). Deformation zone is characterized by horizontal shortening accommodated by thrust faults and folding. Thin layers of drape above the zone indicates the deformation is not part of the landslide deposit (i.e., run-out blocks and debris) but rather in situ deformation induced by impact of the landslide.

the ratio of horizontal to vertical stress should be in the range of 0.2–0.4 (Lambe & Whitman, 1969). The Biot coefficient α is assumed to be 1 (Engelder & Fischer, 1994; Nur & Byerlee, 1971).

$$P_f = \rho_w g D_w + \rho_w g z \tag{1}$$

$$\sigma^0_{zz} = -\rho_s g z - \rho_w g D_w + P_f \tag{2}$$

$$\sigma^0_{xx} = \frac{\nu}{1-\nu}\sigma^0_{zz} - \alpha\left(\frac{1-2\nu}{1-\nu}\right)\rho_w g z \tag{3}$$

Normal $\tau_n(x)$ and shear $\tau_s(x)$ tractions exerted on the ocean bottom by the landslide blocks are applied along the line $z = 0, -a \le x \le a$ (Figure 2a). All calculations assume plane strain ($\epsilon_y = 0$). The overburden stress due to the overlying landslide blocks ($\tau_n = \rho_{bl} h g$) is approximated as 1.9 MPa, calculated by multiplying the drained bulk density of the landslide blocks (ρ_{bl}), approximate height of the landslide blocks (h) of 235-m, and gravitational acceleration (g) (Lenz et al., 2019). The shear traction due to the decelerating landslide blocks ($\tau_s = -\mu_s \tau_n$) is calculated by multiplying the static basal friction coefficient μ_s by the pressure of the overlying landslide blocks.

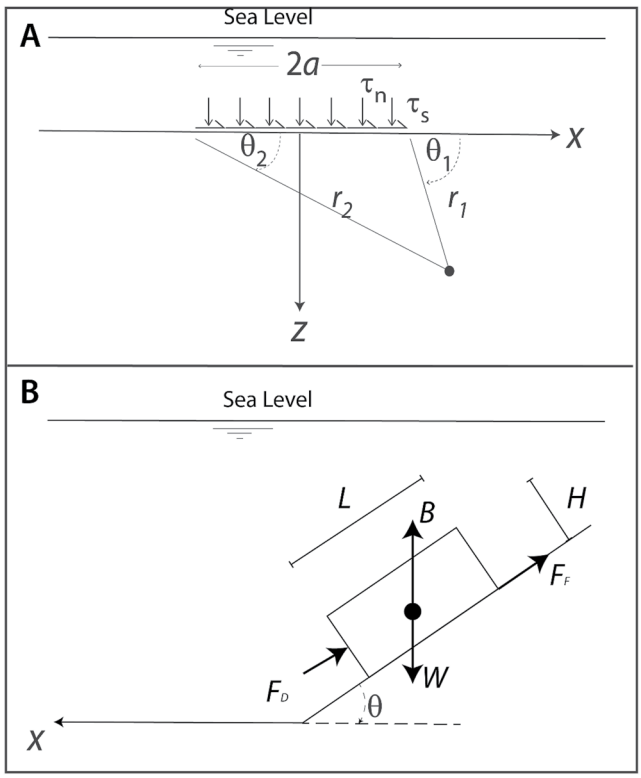

Figure 2. Idealized models used in this study. (a) Finite length line load on an undrained, poroelastic half space. Boundary value problem is solved in a bi-polar coordinate system with coordinates r_1, r_2, θ_1, and θ_2, as defined in Equations 4–6, following Johnson (1985). Half space surface is located 3,000 m beneath local sea level. (b) Frictional block model of slide transport using a modified approach from Hürlimann et al. (2000) with a ramp-flat geometry consistent with the 44-N slide path.

Note that the basal friction coefficient is static, used to approximate the frictional tractions associated with landslide block cessation.

The perturbed stresses due to tractions τ_n and τ_s are calculated throughout the model domain according to Johnson (1985):

$$\Delta\sigma_{zz} = -\frac{\tau_n}{2\pi}\{2(\theta_1-\theta_2)+(\sin 2\theta_1-\sin 2\theta_2)\} + \frac{\tau_s}{2\pi}\{\cos 2\theta_1-\cos 2\theta_2\} \quad (4)$$

$$\Delta\sigma_{xx} = -\frac{\tau_n}{2\pi}\{2(\theta_1-\theta_2)+(\sin 2\theta_1-\sin 2\theta_2)\} + \frac{\tau_s}{2\pi}\{4\ln(r_1/r_2)-(\cos 2\theta_1-\cos 2\theta_2)\} \quad (5)$$

$$\Delta\sigma_{xz} = \frac{\tau_n}{2\pi}\{\cos 2\theta_1-\cos 2\theta_2\} - \frac{\tau_s}{2\pi}\{2(\theta_1-\theta_2)+(\sin 2\theta_1-\sin 2\theta_2)\} \quad (6)$$

where $\theta_1, \theta_2 = \tan^{-1}(z/(x \mp a))$ and $r_1, r_2 = \left\{(x \mp a)^2 + z^2\right\}^{1/2}$.

We calculate the total stress state σ_{ij}^T throughout the model domain by taking the sum of the background stresses and the stress perturbation ($\sigma_{ij}^T = \sigma_{xx}^0 + \Delta\sigma_{ij}$). We use two criteria to evaluate the relationship between prescribed surface tractions in the model and observed deformation in the deformed sediments. First, we determine the size of the zone in which the maximum shear stress $\sigma_s^{\max}$ exceeds the undrained shear strength S_u of the sediments (assumed to be $S_u = 0.5\sigma_{zz}^T$, Sawyer & DeVore, 2015). We furthermore determine the orientation of the principal stresses, ensuring the direction of the greatest compressive stress is consistent with principal shortening direction (i.e., sub-horizontal) observed in the deformed sediments. Because the frictional resistance between the block and ocean bottom sediments is a source of substantial uncertainty, we choose values that encompass the full spectrum of possible static values (e.g., Byerlee, 1978; Hornbach et al., 2015; Ikari & Kopf, 2011), including $\mu_s = 0.0$, 0.2, 0.4, and 0.6. While non-physical, the choice of $\mu_s = 0.0$ is a "weak fault" endmember that results in zero shear tractions.

2.2. Mechanical Slide Model to Estimate the Dynamic Behavior of the 44-N Slide

We also take a complementary approach to independently confirm the physical feasibility of rapid transport of the slide blocks. We adapted the model of Hürlimann et al. (2000) that idealizes landslide blocks as a single rigid block with constant density and dimensions (see Text S1 in Supporting Information S1). Instead, we employ ramp-flat geometry matching the drop height and average slope of the N-44 slide (Lenz et al., 2019). We use dimensions of the largest block observed in the two-dimensional seismic profile measured to be approximately 2,300 long, 3,200 wide, and 410-m high (Figure 1). We also account for forces experienced as the block moves downslope and transitions out into the abyssal plane (Figure 2b). L and H are the length and the height of the sliding block respectively, B is the buoyant force, W is the force from the mass of the blocks, F_F is the frictional force, F_D is the drag force, and θ is the slope angle, taken here to be 12.8°. Dynamic coefficients of friction (μ_d) relevant to F_F are expected to be less than 0.1 (Garcia et al., 1994; Ui, 1983). In the model, F_D drops to zero when the Froude number, Fr, exceeds 0.4, which was shown in laboratory experiments as the minimum Froude number required to produce hydroplaning (Mohrig et al., 1999). Details of the model can be found in Hürlimann et al. (2000) and in Supporting Information S1.

3. Results

3.1. Subsurface Stresses Resulting From Line Load

Calculations using Equations 4–6 demonstrate a systematic relationship between basal friction and the expected subsurface instability zone (Figure 3). For $\mu_s = 0$, a small region less than 100 deep and 100 m wide is destabilized

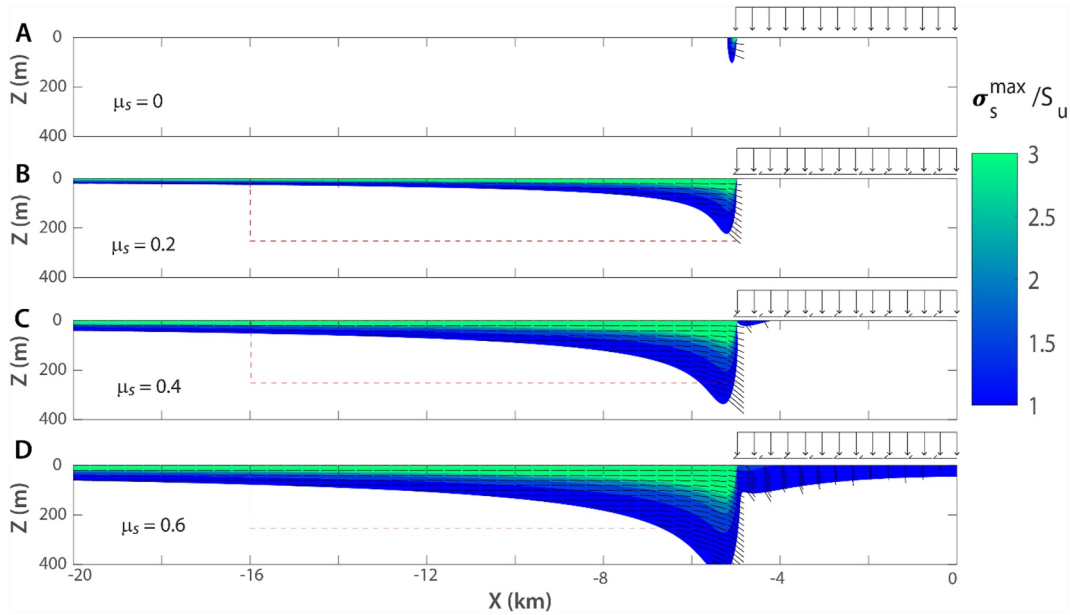

Figure 3. Max shear stress (σ_s^{max}) divided by the in situ strength (S_u) for $\tau_n = 1.9$ MPa and (a) $\tau_s = 0.0\ \tau_n$, (b) $\tau_s = 0.2\ \tau_n$, (c) $\tau_s = 0.4\ \tau_n$, and (d) $\tau_s = 0.6\ \tau_n$ over the domain $-2a \le x \le 0$, where the center of the N-44 slide is located at $x = 0$. Normal $\tau_n(x)$ and shear $\tau_s(x)$ traction distributions and are shown schematically on the upper right-hand corner of each plot. Filled contours are shown only for $\sigma_s^{max}/S_u \ge 1$ (i.e., for regions of the domain that are critically stressed for failure). Overlain on each plot are directions of max compressive stress (σ_1) shown by black dashed lines, which should be approximately coincident with the shortening direction as inferred from the fold and thrust kinematics. Red dashed box is 11 km long and 250 m high, coincident with the inferred original size of deformed sediment package. All figures have approximately 5× vertical exaggeration.

(Figure 3a). In contrast, for all nonzero static friction cases (Figures 3b and 3c), sediments within a few tens of meters of the ocean bottom become critically stressed across the entire domain, from the western terminus of the N-44 slide blocks at $x = -5$ km to a distance 15 km to the west (Figure 3b). The maximum depth of the activated domain, proximal to the slide terminus, increases with increasing μ_s, exceeding 400 m depth for the case of $\mu_s = 0.6$ (Figures 3b–3d). For each case, stress trajectories are consistent with horizontal shortening throughout the sediments.

Because these calculations assume infinitesimal strain, the stress fields can only reasonably be compared to the expected conditions at the initiation of deformation within the ocean bottom sediments. In Figures 3b and 3c, the red dashed box indicates the approximate cross-sectional area (11 km × 250 m) of sediments before shortening. For all cases of non-negligible friction, sediments are destabilized across the entire horizontal domain. It is difficult to discriminate between μ_s of 0.2, 0.4, and 0.6, but, importantly, these results demonstrate that a non-negligible shear traction between the blocks and sediments is required, which would not be expected if the slide is simply creeping along a sub-horizontal ocean bottom due to high fluid pressures.

3.2. Slide Transport Model

Slide transport calculations are shown in Figure 4 for dynamic friction coefficients $\mu_d = 0.05, 0.1, 0.2$. For each simulation, slide velocity accelerates rapidly at the onset of slip (Figure 4a). For the case of $\mu_d = 0.2$, acceleration slows progressively until the block reaches the bottom of the slope, after which the slide rapidly decelerates and stops only a short distance from the base of the slope at ~5,500 m. This slide never experiences hydroplaning, and the dynamic friction coefficient remains at 0.2 for the entire slide period. Peak slide velocity for $\mu_d = 0.2$ is approximately 20 m/s (Figure 4a), and slide duration is approximately 400 s (Figure 4b). For the cases of $\mu_d = 0.05$ and 0.1, the slide accelerates a short distance, and slightly above speed of 20 m/s, the Froude number reaches 0.4 (Figure 4c), causing hydroplaning (Figure 4d), and sudden acceleration (Figure 4a). Slide acceleration continues, but slows, until the base of the slope. After reaching a peak speed of approximately 60 m/s in both cases, the slide block begins to decelerate upon reaching the abyssal plain. The slides continue to decelerate until

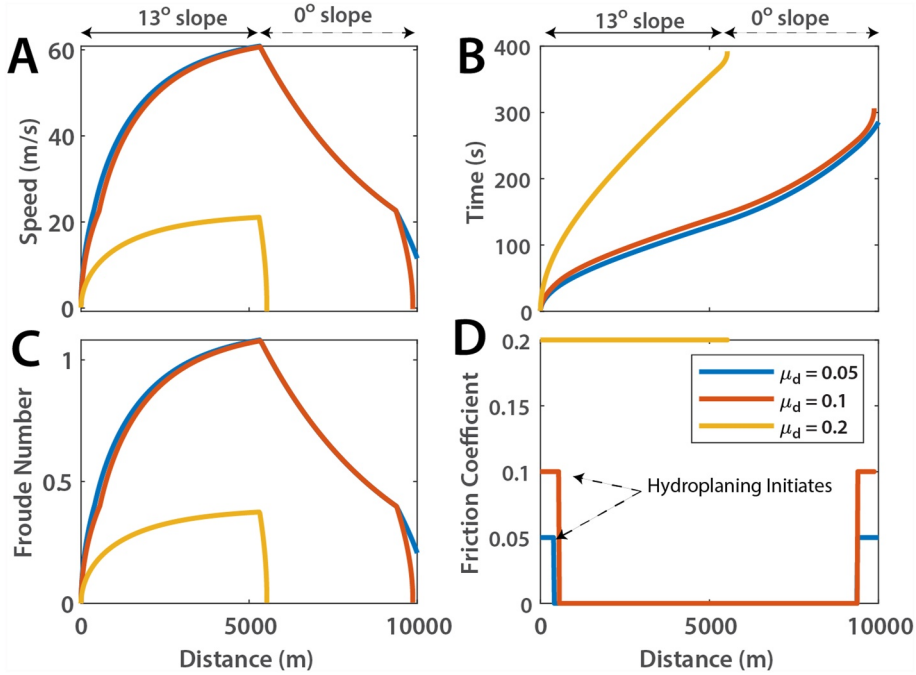

Figure 4. (a) Landslide speed versus distance for three choices of dynamic friction coefficient, $\mu_d = 0.05$, 0.1, 0.2. Arrows along top of plot indicate break in slope that occurs at approximately 5,300 m, after the initial drop along a slope of 13° to abyssal plain, with 0° slope. (b) Time versus distance for each case. (c) Froude number versus distance. Hydroplaning occurs when the velocity is high enough to allow buoyancy forces to uplift landslide block causing it to lose contact with the surface. Slide as frictionless when the Froude number exceeds this threshold. (d) Evolution of friction coefficient with distance. Friction drops to zero when hydroplaning initiates, and strength recovers when Froude number falls below 0.4. For $\mu_d = 0.2$, frictional resistance remains constant for entire simulation, because Froude number never exceeds 0.4.

the Froude number falls below 0.4, after which the slide rapidly decelerates due to frictional drag. The final slide distance is 9,900 and 10,200 m (Figure 4a) for $\mu_d = 0.05$ and 0.1, respectively. These distances are both within the observed range of horizontal transport distances (Figure 1).

4. Discussion and Implications

A key result of this analysis is that to explain where the slide mass came to rest, the 44-N slide must have had significant momentum (peak speeds up to 60 m/s), which is consistent with a fast-moving slide; not a creeping slide. By comparison, one of the most well-studied submarine landslides, the Storegga Slide, produced a very large tsunami (Bondevik, 2003; Bondevik et al., 2005; Harbitz, 1992). Modeled maximum velocity for the Storegga Slide are 35–60 m/s (De Blasio et al., 2003; Løvholt et al., 2017). The Storegga Slide geomorphology was very different from the 44-N Slide because the Storegga Slide disintegrated upon failure (Berg et al., 2005; Bryn et al., 2005; Kvalstad et al., 2005; Løvholt et al., 2005). The 44-N slide may be more similar to the blockier Trænadjupet Slide also offshore Norway (Laberg & Vorren, 2000). The Trænadjupet Slide may have also generated a tsunami, although recent modeling suggests it was smaller than the Storegga tsunami (Løvholt et al., 2017). While the exact physics of simulating a potential tsunami are beyond the scope of this paper, it is possible that the 44-N Slide could produce a tsunami.

The fact that the 44-N slide blocks retained their shape after traveling 1,200-m vertically down a steep 13° slope and up to 10-km horizontally out into the abyssal plain with enough force to induce a large deformation zone has previously been difficult to explain. Undrained shear strength collected on Ocean Drilling Program Leg 146 at Site 892 (Westbrook et al., 1994), approximately 80 km north along strike from the 44-N slide head scarp, shows the sediments that make up the slopes in this part of the margin are relatively strong (Lenz et al., 2019) compared to normally consolidated sediments (Lambe & Whitman, 1969). The enhanced strength

is similar to other strength profiles observed in seismically active areas (Sawyer & DeVore, 2015). Stronger sediments are more likely to remain intact during slope failure, such as those observed in natural (McAdoo & Watts, 2004; Tappin et al., 2002; Watts, 2004) and experimental settings (Sawyer et al., 2012; Silver & Dugan, 2020). Evidence of the existence of gas hydrates was also observed via bottom simulating reflectors in reflection seismic data along this entire margin (Phrampus et al., 2018; Tréhu & Phrampus, 2022). Given that gas hydrates have been known to enhance sediment cohesion (Waite et al., 2009) it may be possible that gas hydrates could aid in keeping this deposit intact. Finally, hydroplaning has also been used to explain how submarine landslides have such long runouts and, in some cases, remain intact throughout the process (De Blasio et al., 2004; Elverhoi et al., 2010; Mohrig et al., 1999). A combination of the landslide occurring along a steep slope with relatively strong sediments with hydroplaning during transport could explain how the blocks retained the large dimensions and sharp angles, as well as supports our conclusion of high speeds and tsunamigenic potential of the blocks.

The models herein are highly idealized and are thus not expected to be exact reproductions of the complex processes involved in the initiation and transport of the 44-N slide, nor the fold and thrust style deformation of sediments at the slide terminus. Ocean sediments are neither perfectly elastic, isotropic, or homogeneous, the process of fold-and-thrust style deformation can be achieved by non-unique kinematic pathways and is not likely volume conserving, and the coefficient of friction throughout the processes of slip initiation, acceleration, and cessation is not constant. Furthermore, we ignore in our idealized transport models the effect of complex initiation mechanisms such as retrogressive sliding (Kvalstad et al., 2005; Løvholt et al., 2017). Despite these idealizations, both modeling approaches independently confirm two key observations of the deformation that occurred during the 44-N slide. First, calculations idealizing the load imparted by the slide blocks on the ocean bottom reproduce both the general dimensions of the initial deformation zone for coefficients of static friction across the range $\mu_s = 0.2$–0.6, although the thickness of the deformed package is likely most consistent with static friction at or above the higher end. Furthermore, the stress trajectories in the activated zone within the ocean sediments are consistent with the inferred overall kinematics of the deformed sediments. Second, for coefficients of dynamic friction between $\mu_d = 0.05$ and 0.1, the total slide distance of approximately 10 km is within the observed range of horizontal transport for the N-44 slide.

5. Conclusion

Impact-induced deformation from submarine landslides can be related quantitatively to the dynamics of the landslide. The 44-N slide along the Cascadia Subduction Zone, recently imaged with multi-channel seismic data, created a large impact zone in the seafloor sediments as a result of impact forces. The deformation zone scale is consistent with impact forces induced by the landslide as it came to rest on the nearly flat seafloor and is not the result of slow, creep-like deformation. Maximum speeds of 60 m/s and hydroplaning may have facilitated the long run-out distance and aid in keeping the blocks largely intact throughout the process. It is not clear if the 44-N slide generated a tsunami, but the dynamics suggested by this analysis are within the range of past known tsunamigenic slide events. The Cascadia margin is capable of producing large-magnitude earthquakes which could facilitate future fast-moving blocky slides; therefore, this result informs hazards analyses of the potential slide dynamics that are capable along this margin. Globally, this method can be applied to other analyses of slides where deformation zones can be sufficiently imaged in modern settings or outcrops. In fact, the 44-N Slide is not unique to this margin. There have been at least five other similar events indicated along the south-central Cascadia Subduction Zone (Tréhu et al., 2022). Additionally, we would expect to find similar in situ deformation where large blocky slides are common such as other subduction zones, volcanic islands, and margins affected by salt diapirism (Alves, 2015).

Data Availability Statement

The reflection seismic data analyzed during the current study can be accessed publicly from the Marine Geoscience Data System (MGDS) website, https://www.marine-geo.org/tools/entry/RR1718. The MATLAB scripts used to perform the data analysis are archived with Zenodo here: https://doi.org/10.5281/zenodo.8212224.

Acknowledgments
BLL and DES thank the US National Science Foundation-funded UNOLS Early Career Seismic Chief Scientist Training Cruise 1,718 scientists and crew. WAG received support from National Science Foundation under Grant 2113155. DES received support from National Science Foundation under award 1945543. The authors kindly thank Jeffrey Obelcz and Matt Ikari for constructive reviews that improved the manuscript.

References

Alves, T. M. (2015). Submarine slide blocks and associated soft-sediment deformation in deep-water basins: A review. *Marine and Petroleum Geology*, *67*, 262–285. https://doi.org/10.1016/j.marpetgeo.2015.05.010

Berg, K., Solheim, A., & Bryn, P. (2005). The Pleistocene to recent geological development of the Ormen Lange area. In *Ormen lange–an integrated study for safe field development in the storegga submarine area* (pp. 45–56).

Bondevik, S. (2003). Storegga tsunami sand in peat below the Tapes beach ridge at Harøy, western Norway, and its possible relation to an early Stone Age settlement. *Boreas*, *32*(3), 476–483. https://doi.org/10.1111/j.1502-3885.2003.tb01229.x

Bondevik, S., Løvholt, F., Harbitz, C., Mangerud, J., Dawson, A., & Svendsen, J. I. (2005). The Storegga slide tsunami—Comparing field observations with numerical simulations. In *Ormen lange–an integrated study for safe field development in the Storegga submarine area* (pp. 195–208). Elsevier.

Bryn, P., Berg, K., Forsberg, C. F., Solheim, A., & Kvalstad, T. J. (2005). Explaining the Storegga slide. *Marine and Petroleum Geology*, *22*(1–2), 11–19. https://doi.org/10.1016/j.marpetgeo.2004.12.003

Byerlee, J. (1978). Friction of rocks. *Rock Friction and Earthquake Prediction*, *116*(4–5), 615–626. https://doi.org/10.1007/BF00876528

De Blasio, F. V., Engvik, L., Harbitz, C. B., & Elverhøi, A. (2004). Hydroplaning and submarine debris flows. *Journal of Geophysical Research*, *109*(C1), C01002. https://doi.org/10.1029/2002JC001714

De Blasio, F. V., Issler, D., Elverhøi, A., Harbitz, C. B., Ilstad, T., Bryn, P., et al. (2003). Dynamics, velocity and run-out of the giant Storegga slide. In *Submarine mass movements and their consequences* (pp. 223–230). Springer.

Elverhoi, A., Breien, H., De Blasio, F. V., Harbitz, C. B., & Pagliardi, M. (2010). Submarine landslides and the importance of the initial sediment composition for run-out length and final deposit. *Ocean Dynamics*, *60*(4), 1027–1046. https://doi.org/10.1007/s10236-010-0317-z

Engelder, T., & Fischer, M. P. (1994). Influence of poroelastic behavior on the magnitude of minimum horizontal stress, S_h in overpressured parts of sedimentary basins. *Geology*, *22*(10), 949–952. https://doi.org/10.1130/0091-7613(1994)022<0949:IOPBOT>2.3.CO;2

Fine, I. V., Rabinovich, A. B., Bornhold, B. D., Thomson, R. E., & Kulikov, E. A. (2005). The Grand Banks landslide-generated tsunami of November 18, 1929: Preliminary analysis and numerical modeling. *Marine Geology*, *215*(1–2), 45–57. https://doi.org/10.1016/j.margeo.2004.11.007

Garcia, L., Diez-Gil, J. L., & Arana, V. (1994). A large volcanic debris avalanche in the Pliocene Roque Nublo stratovolcano, Gran Canaria, Canary Islands. *Journal of Volcanology and Geothermal Research*, *63*(3–4), 217–229. https://doi.org/10.1016/0377-0273(94)90075-2

Goldfinger, C., Galer, S., Beeson, J., Hamilton, T., Black, B., Romsos, C., et al. (2017). The importance of site selection, sediment supply, and hydrodynamics: A case study of submarine paleoseismology on the northern Cascadia margin, Washington USA. *Marine Geology*, *384*, 4–46. https://doi.org/10.1016/j.margeo.2016.06.008

Goldfinger, C., Kulm, L. D., McNeill, L. C., & Watts, P. (2000). Super-scale failure of the southern Oregon Cascadia margin. *Pure and Applied Geophysics*, *157*(6), 1189–1226. https://doi.org/10.1007/s000240050023

Goldfinger, C., Nelson, C. H., Morey, A. E., Johnson, J. E., Patton, J. R., Karabanov, E. B., et al. (2012). *Turbidite event history—Methods and implications for Holocene paleoseismicity of the Cascadia subduction zone*. (No. 1661-F). US Geological Survey. https://doi.org/10.3133/pp1661F

Grilli, S. T., & Watts, P. (2005). Tsunami generation by submarine mass failure. I: Modeling, experimental validation, and sensitivity analyses. *Journal of Waterway, Port, Coastal, and Ocean Engineering*, *131*(6), 283–297. https://doi.org/10.1061/(asce)0733-950x(2005)131:6(283)

Hampton, M. A., Lee, H. J., & Locat, J. (1996). Submarine landslides. *Reviews of Geophysics*, *34*(1), 33–59. https://doi.org/10.1029/95RG03287

Harbitz, C. B. (1992). Model simulations of tsunamis generated by the Storegga slides. *Marine Geology*, *105*(1–4), 1–21. https://doi.org/10.1016/0025-3227(92)90178-K

Harbitz, C. B., Løvholt, F., & Bungum, H. (2014). Submarine landslide tsunamis: How extreme and how likely? *Natural Hazards*, *72*(3), 1341–1374. https://doi.org/10.1007/s11069-013-0681-3

Haugen, K. B., Løvholt, F., & Harbitz, C. B. (2005). Fundamental mechanisms for tsunami generation by submarine mass flows in idealised geometries. *Marine and Petroleum Geology*, *22*(1–2), 209–217. https://doi.org/10.1016/j.marpetgeo.2004.10.016

Hill, J. C., Watt, J. T., & Brothers, D. S. (2022). Mass wasting along the Cascadia subduction zone: Implications for abyssal turbidite sources and the earthquake record. *Earth and Planetary Science Letters*, *597*, 117797. https://doi.org/10.1016/j.epsl.2022.117797

Hornbach, M. J., Manga, M., Genecov, M., Valdez, R., Miller, P., Saffer, D., et al. (2015). Permeability and pressure measurements in Lesser Antilles submarine slides: Evidence for pressure-driven slow-slip failure. *Journal of Geophysical Research: Solid Earth*, *120*(12), 7986–8011. https://doi.org/10.1002/2015JB012061

Howarth, J. D., Orpin, A. R., Kaneko, Y., Strachan, L. J., Nodder, S. D., Mountjoy, J. J., et al. (2021). Calibrating the marine turbidite palaeoseismometer using the 2016 Kaikōura earthquake. *Nature Geoscience*, *14*(3), 161–167. https://doi.org/10.1038/s41561-021-00692-6

Hürlimann, M., Garcia-Piera, J. O., & Ledesma, A. (2000). Causes and mobility of large volcanic landslides: Application to Tenerife, Canary Islands. *Journal of Volcanology and Geothermal Research*, *103*(1–4), 121–134. https://doi.org/10.1016/S0377-0273(00)00219-5

Ikari, M. J., & Kopf, A. J. (2011). Cohesive strength of clay-rich sediment. *Geophysical Research Letters*, *38*(16), L16309. https://doi.org/10.1029/2011GL047918

Jiang, L., & LeBlond, P. H. (1992). The coupling of a submarine slide and the surface waves which it generates. *Journal of Geophysical Research*, *97*(C8), 12731–12744. https://doi.org/10.1029/92JC00912

Johnson, K. L. (1985). *Contact mechanics* (pp. 11–14). Cambridge University Press.

Kawata, Y., Benson, B. C., Borrero, J. C., Borrero, J. L., Davies, H. L., de Lange, W. P., et al. (1999). Tsunami in Papua New Guinea was as intense as first thought. *Eos, Transactions American Geophysical Union*, *80*(9), 101–105. https://doi.org/10.1029/99EO00065

Kioka, A., Schwestermann, T., Moernaut, J., Ikehara, K., Kanamatsu, T., Eglinton, T. I., & Strasser, M. (2019). Event stratigraphy in a hadal oceanic trench: The Japan trench as sedimentary archive recording recurrent giant subduction zone earthquakes and their role in organic carbon export to the deep sea. *Frontiers in Earth Science*, *7*, 319. https://doi.org/10.3389/feart.2019.00319

Kvalstad, T. J., Andresen, L., Forsberg, C. F., Berg, K., Bryn, P., & Wangen, M. (2005). The Storegga slide: Evaluation of triggering sources and slide mechanics. In *Ormen lange–an integrated study for safe field development in the storegga submarine area* (pp. 245–256).

Laberg, J. S., & Vorren, T. O. (2000). The Trænadjupet slide, offshore Norway — Morphology, evacuation and triggering mechanisms. *Marine Geology*, *171*(1–4), 95–114. https://doi.org/10.1016/S0025-3227(00)00112-2

Lambe, T. W., & Whitman, R. V. (1969). Soil mechanics (p. 553).

Lenz, B. L., & Sawyer, D. E. (2021). Mass transport deposits in reflection seismic data offshore Oregon. *USA, Basin Research*, *34*(1), 81–98. https://doi.org/10.1111/bre.12611

Lenz, B. L., Sawyer, D. E., Phrampus, B., Davenport, K., & Long, A. (2019). Seismic imaging of seafloor deformation induced by impact from large submarine landslide blocks, offshore Oregon. *Geosciences*, *9*(1), 10. https://doi.org/10.3390/geosciences9010010

Locat, J., & Lee, H. J. (2002). Submarine landslides: Advances and challenges. *Canadian Geotechnical Journal*, *39*(1), 193–212. https://doi.org/10.1139/t01-089

Løvholt, F., Bondevik, S., Laberg, J. S., Kim, J., & Boylan, N. (2017). Some giant submarine landslides do not produce large tsunamis. *Geophysical Research Letters*, *44*(16), 8463–8472. https://doi.org/10.1002/2017gl074062

Løvholt, F., Harbitz, C. B., & Haugen, K. B. (2005). A parametric study of tsunamis generated by submarine slides in the Ormen Lange/Storegga area off western Norway. In *Ormen lange–an integrated study for safe field development in the storegga submarine area* (pp. 219–231). Elsevier.

Løvholt, F., Schulten, I., Mosher, D., Harbitz, C., & Krastel, S. (2019). *Modelling the 1929 Grand Banks slump and landslide tsunami*. Geological Society, London, Special Publications. https://doi.org/10.1144/SP477.28

Masson, D. G., Harbitz, C. B., Wynn, R. B., Pedersen, G., & Løvholt, F. (2006). Submarine landslides: Processes, triggers and hazard prediction. *Philosophical Transactions of the Royal Society A: Mathematical, Physical & Engineering Sciences*, *364*(1845), 2009–2039. https://doi.org/10.1098/rsta.2006.1810

McAdoo, B. G., Pratson, L. F., & Orange, D. L. (2000). Submarine landslide geomorphology, US continental slope. *Marine Geology*, *169*(1–2), 103–136. https://doi.org/10.1016/S0025-3227(00)00050-5

McAdoo, B. G., & Watts, P. (2004). Tsunami hazard from submarine landslides on the Oregon continental slope. *Marine Geology*, *203*(3–4), 235–245. https://doi.org/10.1016/S0025-3227(03)00307-4

McCaffrey, R., King, R. W., Payne, S. J., & Lancaster, M. (2013). Active tectonics of northwestern U.S. inferred from GPS-derived surface velocities. *Journal of Geophysical Research: Solid Earth*, *118*(2), 709–723. https://doi.org/10.1029/2012jb009473

McHugh, C. M., Kanamatsu, T., Seeber, L., Bopp, R., Cormier, M. H., & Usami, K. (2016). Remobilization of surficial slope sediment triggered by the A.D. 2011 Mw 9 Tohoku-Oki earthquake and tsunami along the Japan. *Trench: Geology*, *44*(5), 391–394. https://doi.org/10.1130/g37650.1

Mohrig, D., Elverhøi, A., & Parker, G. (1999). Experiments on the relative mobility of muddy subaqueous and subaerial debris flows, and their capacity to remobilize antecedent deposits. *Marine Geology*, *154*(1–4), 117–129. https://doi.org/10.1016/S0025-3227(98)00107-8

Mountjoy, J. J., Howarth, J. D., Orpin, A. R., Barnes, P. M., Bowden, D. A., Rowden, A. A., et al. (2018). Earthquakes drive large-scale submarine canyon development and sediment supply to deep-ocean basins. *Science Advances*, *4*(3), eaar3748. https://doi.org/10.1126/sciadv.aar3748

Muhari, A., Imamura, F., Arikawa, T., Hakim, A. R., & Afriyanto, B. (2018). Solving the puzzle of the September 2018 Palu, Indonesia, tsunami mystery: Clues from the tsunami waveform and the initial field survey data. *Journal of Disaster Research*, *13*(Scientific Communication), sc20181108. https://doi.org/10.20965/jdr.2018.sc20181108

Nur, A., & Byerlee, J. (1971). An exact effective stress law for elastic deformation of rock with fluids. *Journal of Geophysical Research*, *76*(26), 6414–6419. https://doi.org/10.1029/JB076i026p06414

Pakoksung, K., Suppasri, A., Imamura, F., Athanasius, C., Omang, A., & Muhari, A. (2019). Simulation of the submarine landslide tsunami on 28 September 2018 in Palu Bay, Sulawesi Island, Indonesia, using a two-layer model. *Pure and Applied Geophysics*, *176*(8), 3323–3350. https://doi.org/10.1007/s00024-019-02235-y

Phrampus, B., Tominaga, M., Trehu, A., & Lyle, M. W. (2018). *Multi-channel seismic processed data offshore Oregon, acquired by the R/V Roger Revelle in 2017 (RR1718)*. Interdisciplinary Earth Data Alliance (IEDA).

Rowe, C. D., & Griffith, W. A. (2015). Do faults preserve a record of seismic slip: A second opinion. *Journal of Structural Geology*, *78*, 1–26. https://doi.org/10.1016/j.jsg.2015.06.006

Ryan, W. B. F., Carbotte, S. M., Coplan, J. O., O'Hara, S., Melkonian, A., Arko, R., et al. (2009). Global multi resolution topography synthesis. *Geochemistry, Geophysics, Geosystems*, *10*(3), Q03014. https://doi.org/10.1029/2008GC002332

Sawyer, D. E., & DeVore, J. R. (2015). Elevated shear strength of sediments on active margins: Evidence for seismic strengthening. *Geophysical Research Letters*, *42*(23), 10–216. https://doi.org/10.1002/2015GL066603

Sawyer, D. E., Flemings, P. B., Buttles, J., & Mohrig, D. (2012). Mudflow transport behavior and deposit morphology: Role of shear stress to yield strength ratio in subaqueous experiments. *Marine Geology*, *307*, 28–39. https://doi.org/10.1016/j.margeo.2012.01.009

Shipboard Scientific Party. (1973). Site 174. In *Deep Sea drilling project; DSDP initial reports* (Vol. 18, pp. 97–167). DSDP. https://doi.org/10.2973/dsdp.proc.18.1973

Shipboard Scientific Party. (1994). Site 892. In G. K. Westbrook, B. Carson, & R. J. Musgrave, J. Ashi, B. Baranov, K. M. Brown, et al. (Eds.) *Proc. ODP, initial reports* (Vol. 146, No. (1), pp. 301–378). Ocean Drilling Program. https://doi.org/10.2973/odp.proc.ir.146-1.010.1994

Silver, M. M. W., & Dugan, B. (2020). The influence of clay content on submarine slope failure: Insights from laboratory experiments and numerical models. *Geological Society, London, Special Publications*, *500*(1), 301–309. https://doi.org/10.1144/SP500-2019-186

Tappin, D. R., Watts, P., McMurtry, G. M., Lafoy, Y., & Matsumoto, T. (2002). Prediction of slump generated tsunamis: The July 17th 1998 Papua New Guinea event. *Science of Tsunami Hazards*, *20*(4), 222–238.

ten Brink, U. (2009). Tsunami hazard along the US Atlantic coast. *Marine Geology*, *264*(1–2), 1–3. https://doi.org/10.1016/j.margeo.2009.03.011

Tinti, S., Bortolucci, E., & Chiavettieri, C. (2001). Tsunami excitation by submarine slides in shallow-water approximation. *Pure and Applied Geophysics*, *158*(4), 759–797. https://doi.org/10.1007/pl00001203

Tréhu, A. M., & Phrampus, B. J. (2022). Accretionary wedge tectonics and gas hydrate distribution in the Cascadia forearc. In J. Mienert, C. Berndt, A. M. Tréhu, A. Camerlenghi, & C. S. Liu (Eds.), *World atlas of submarine gas hydrates in continental margins*. Springer. https://doi.org/10.1007/978-3-030-81186-0_9

Tréhu, A. M., Tominaga, M., Lyle, M., Davenport, K., Phrampus, B. J., Favorito, J., et al. (2022). The hidden history of the southsouth-central Cascadia subduction zone recorded on the Juan de Fuca plate offshore southwest Oregon. *Geochemistry, Geophysics, Geosystems*, *23*(9), e2021GC010318. https://doi.org/10.1029/2021gc010318

Ui, T. (1983). Volcanic dry avalanche deposits - Identification and comparison with non volcanic debris stream deposits. *Journal of Volcanology and Geothermal Research*, *18*(1–4), 135–150. https://doi.org/10.1016/0377-0273(83)90006-9

Vanneste, M., Forsberg, C. F., Glimsdal, S., Harbitz, C. B., Issler, D., Kvalstad, T. J., et al. (2013). Submarine landslides and their consequences: What do we know, what can we do? In *Landslide science and practice* (pp. 5–17). Springer.

von Huene, R., Bourgois, J., Miller, J., & Pautot, G. (1989). A large tsunamogenic landslide and debris flow along the Peru Trench. *Journal of Geophysical Research*, *94*(B2), 1703–1714. https://doi.org/10.1029/JB094iB02p01703

Waite, W. F., Santamarina, J. C., Cortes, D. D., Dugan, B., Espinoza, D. N., Germaine, J., et al. (2009). Physical properties of hydrate-bearing sediments. *Reviews of Geophysics*, *47*(4), RG4003. https://doi.org/10.1029/2008RG000279

Wallace, R. E. (1981). Active faults, paleoseismology, and earthquake hazards in the western United States. *Earthquake Prediction: An International Review*, *4*, 209–216.

Walton, M. A. L., Staisch, L. M., Dura, T., Pearl, J. K., Sherrod, B., Gomberg, J., et al. (2021). Toward an integrative geological and geophysical view of Cascadia subduction zone earthquakes. *Annual Review of Earth and Planetary Sciences*, *49*(1), 367–398. https://doi.org/10.1146/annurev-earth-071620-065605

Ward, S. N. (2001). Landslide tsunami. *Journal of Geophysical Research*, *106*(B6), 11201–11215. https://doi.org/10.1029/2000JB900450

Watts, P. (2004). Probabilistic predictions of landslide tsunamis off Southern California. *Marine Geology*, *203*(3–4), 281–301. https://doi.org/10.1016/S0025-3227(03)00311-6

Westbrook, G. K., Carson, B., & Musgrave, R. J. (1994). Leg 146. Introduction: Cascadia margin. In *Proc. ODP, initial reports* (Vol. 146). Ocean Drilling Program. https://doi.org/10.2973/odp.proc.ir.146-1.1994

Yeh, H., Imamura, F., Synolakis, C., Tsuji, Y., Liu, P., & Shi, S. (1993). The Flores island tsunamis. *Eos, Transactions American Geophysical Union*, *74*(33), 369–373. https://doi.org/10.1029/93EO00381

References From the Supporting Information

Heim, A. (1932). *Bergsturz und menschenleben* (No. 20). Fretz & Wasmuth.

Streeter, V., & Wylie, B. (1986). Fluid mechanics (p. 595).